# BIONIC SOLUTION FOR MYASTHENIA GRAVIS

*Bionic Systems Engineering Final Project*

## Analysis of Myasthenia Gravis in the Quadriceps

Agathiya Tharun, Che Jin Goh, Atharva Shetye, Jake Kremer

MAE 263E

Dr. Tyler Clites
clites@ucla.edu

November 19th, 2024

# Section I – Biomechanical Modeling

## A. Pathology: Myasthenia Gravis

Myasthenia Gravis (MG) is a chronic autoimmune disease that affects the neuromuscular junction (NMJ), where nerve impulses communicate with muscles to initiate contraction. The disease occurs when the immune system attacks acetylcholine receptors, reducing their functionality and impairing the ability of nerve impulses to stimulate muscle contraction, as seen in **Figure A.1**.

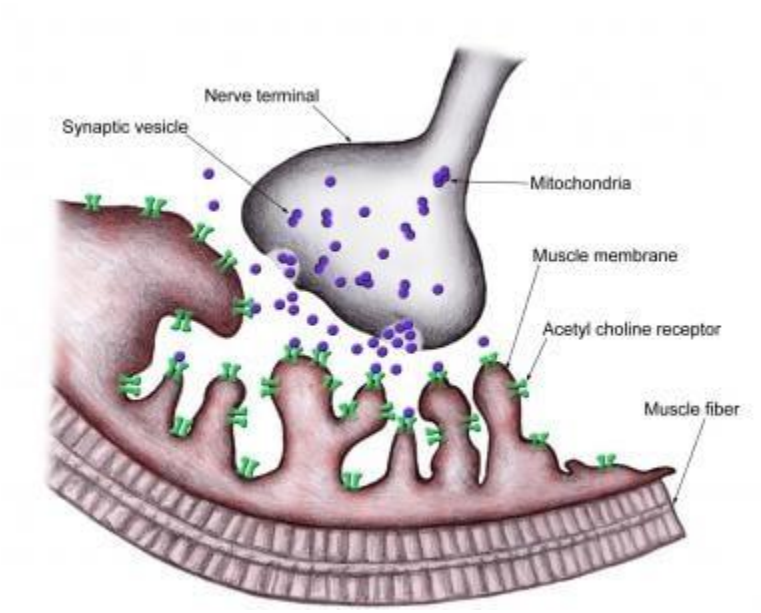


**Figure A.1** Neuromuscular junction site that can be impacted by Myasthenia Gravis

MG can cause significant muscle weakness and, in severe cases, complete loss of muscle function. It primarily impacts skeletal muscles involved in voluntary movement, such as those in the arms, legs, and face. Notably, MG typically affects a muscle group, as the muscles within a group share the same innervation. However, the degree of impact can vary between muscles within the same group, and in some cases, one muscle may be affected while others are spared.

The prevalence of MG is approximately 20 per 100,000 individuals, and it can affect people of all ages and genders. Patients with MG often experience debilitating symptoms, including difficulty walking, maintaining balance, and stabilizing joints. These impairments significantly reduce quality of life, making everyday tasks challenging. Current treatment options include acetylcholinesterase inhibitors to improve communication at the NMJ,

immunosuppressants to reduce immune system activity, and physical therapy to strengthen unaffected muscles. However, these treatments often fail to fully restore functional capacity, especially during high-demand activities like walking.

In this study, the team focuses on how MG affects the vastus muscles within the quadriceps group, specifically targeting the vastus lateralis, vastus medialis, and vastus intermedius. These muscles are critical for knee extension and stabilization during gait. Weakening the vastus muscles disrupts neuromusculoskeletal behavior by reducing knee stability, decreasing stride efficiency, and increasing metabolic cost. This often triggers compensatory mechanisms, such as increased reliance on the rectus femoris or other surrounding muscles, which can lead to further strain and inefficiency in gait mechanics.

MG impacts the vasti muscles by impairing their ability to generate the force necessary for knee extension and stabilization during activities like walking, standing, and climbing stairs. As part of the quadriceps group, the vasti muscles (lateralis, medialis, and intermedius) play a critical role in controlling knee motion, particularly during the stance phase of gait when the knee must bear the body's weight and maintain stability. When MG weakens the vasti muscles, their reduced force production leads to compromised knee stability, which can result in increased joint wobbling or collapse during load-bearing phases. This weakening often triggers compensatory mechanisms from other muscles, such as the rectus femoris, hip extensors, or even passive structures like ligaments, to maintain functional gait. This variability in muscle function exacerbates gait inefficiencies, as the body must adapt to an inconsistent and unbalanced force distribution across the knee joint.

## B. Method of Simulation

To simulate the effects of MG, the team used the OpenSim Gait10dof18musc model and reduced the maximum isometric force of the vasti muscles (vasti_l and vasti_r) by half, from 5000N to 500. This reduction models the weakened force-generating capacity of the vasti, which reflects the impaired neuromuscular function caused by MG. The team ran simulations using Computed Muscle Control (CMC) to evaluate the impact of this pathology on walking mechanics. Key metrics used to assess the simulation include metabolic cost, muscle activation, and peak joint torque. Metabolic cost was analyzed to quantify the energy efficiency of walking, while muscle activation patterns were used to evaluate compensatory behavior, particularly the increased reliance on the rectus femoris. Peak torque at the knee joint was measured to understand the biomechanical consequences of the weakened vasti and to assess how the neuromuscular system adapts to maintain stability and forward progression during gait.

To ensure accurate metabolic cost calculations despite the reduced maximum isometric force, the team recalculated the mass of the vasti muscles. OpenSim's metabolic probes estimate muscle mass using parameters such as maximum isometric force (Fmax), optimal fiber length (Lopt), specific tension, and specific gravity. Because metabolic cost is proportional to muscle mass, which depends on Fmax, lowering Fmax artificially reduces the estimated metabolic expenditure for each unit of activation. To address this, the team calculated the original mass (1.0743 kg) of the vasti muscles using the formula:

$$m = \frac{F_{max}}{Specific\ Tension} \cdot Density \cdot Lm_{opt}$$

The team then fixed this mass in the metabolic probe to prevent it from automatically scaling with the reduced Fmax, ensuring that the metabolic cost estimates accurately reflect the functional behavior of the weakened muscle.

### *B.1 Metabolic Analysis*

As seen in **Figure B.1.1,** the metabolic cost of the rectus femoris (rect_fem_r) is higher in the MG case compared to the healthy case, particularly during late stance (1.6-1.8 seconds). This increase occurs because the rectus femoris compensates for the weakened vasti muscles by taking on a greater role in knee extension. Late stance requires significant effort for propulsion and stabilization, and the rectus femoris, a biarticular muscle, steps in to offset the functional deficit in the vastus. This compensation explains why the MG plot rises sharply during this phase. The slight activity in earlier phases (e.g., around 0.8 seconds) reflects its stabilizing role during swing initiation in the pathological case.

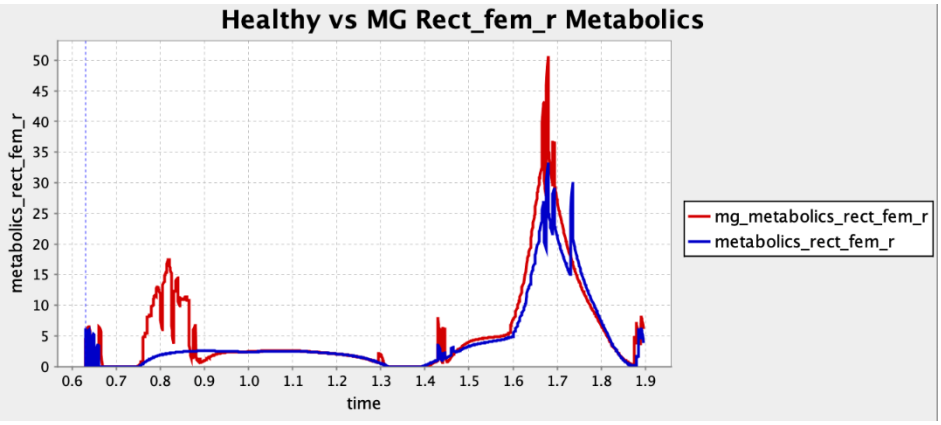


**Figure B.1.1** Comparison between the metabolic cost of the healthy and MG-impacted rectus femoris

As seen in **Figure B.1.2**, the metabolic cost of the vasti muscle (vasti_r) in the MG case peaks during stance phase (around 0.75 seconds), as this phase demands knee stabilization to manage the impact of ground reaction forces. The MG-induced reduction in vasti strength forces the remaining functional capacity to work harder during this critical phase, causing the peak. Beyond heel strike, the metabolic cost of the vasti in the MG case is consistently lower than in the healthy case. This is because the vastus' force-generating capacity has been weakened, resulting in reduced activation and, consequently, lower metabolic demand throughout the rest of the gait cycle.

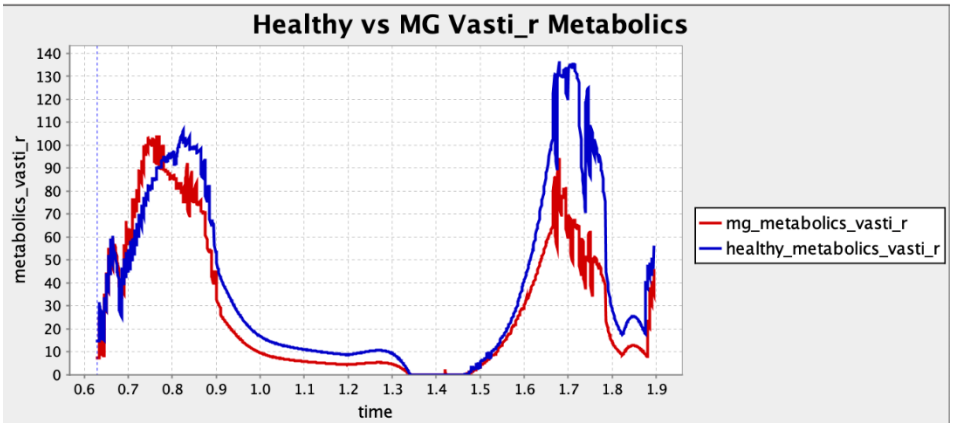


**Figure B.1.2** Comparison between the metabolic cost of the healthy and MG-impacted vasti

In **Figure B.1.3**, the total metabolic cost is slightly lower in the MG case compared to the healthy case. This result reflects the reduced contribution of the weakened vasti muscles, which generate less metabolic demand due to their diminished activity. At the same time, compensatory activation of other muscles, such as the rectus femoris, offsets some of the workload but does not fully restore the energy expenditure of the vasti. Additionally, the absence of an upper body model in OpenSim means that potential compensations from the trunk and arms are unaccounted for, which could also explain why the metabolic cost does not increase as expected. Small fluctuations during heel strike and late stance represent the shifting energy demands across muscle groups as the body adjusts to maintain gait stability.

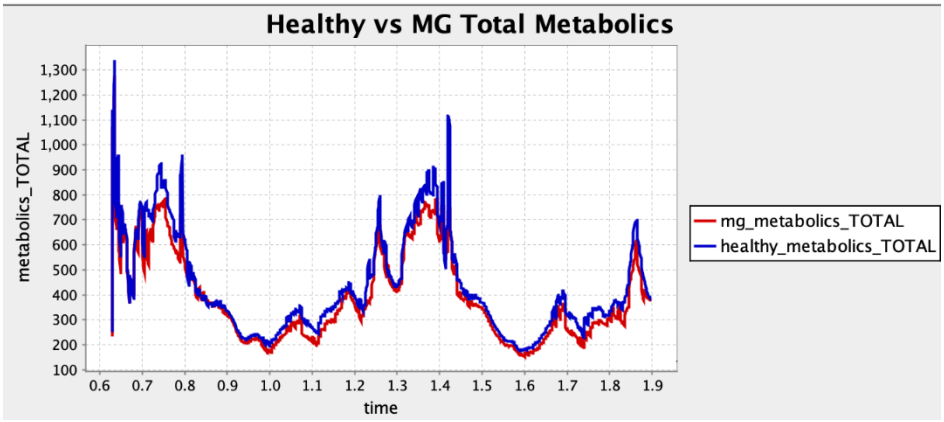


**Figure B.1.3** Comparison between the total metabolic cost of the healthy and MG-impacted bodies

### *B.2 Muscle Activation*

As see in **Figure B.2.1**, the activation of the vasti muscle (vasti_r) is significantly higher in the MG case compared to the healthy case, particularly during heel strike (around 0.7 seconds). This increased activation is expected because, with the maximum isometric force (Fmax) reduced, the vasti require a higher level of activation to produce the necessary force for knee stabilization during this critical phase of the gait cycle. Beyond heel strike, the MG case shows slightly elevated activations during late stance and swing phases, which aligns with the vasti attempting to contribute as much as possible despite their weakened state. However, the reduced Fmax limits their ability to fully engage, leading to periods of lower activation compared to the healthy model.

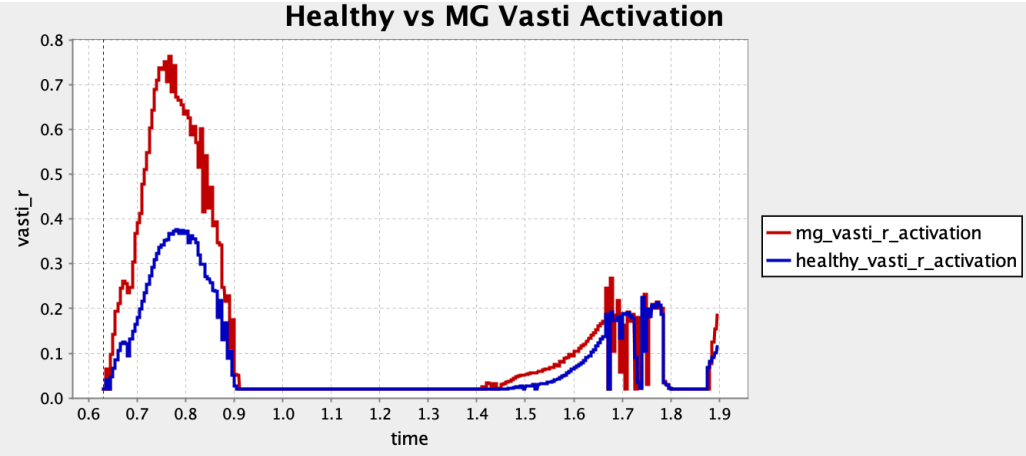


**Figure B.2.1** Comparison between the activation of the healthy and MG-impacted vasti muscles

In **Figure B.2.2**, the rectus femoris (rect_fem_r) activation is noticeably higher in the MG case during late stance (1.6-1.8 seconds). At around 0.8 seconds, the MG case exhibits a noticeable peak in activation, while the healthy case remains near zero activation. This increased activation reflects compensatory behavior, as the rectus femoris takes on a larger role in knee extension to offset the weakened vasti. The spike in activation during this phase highlights the added burden placed on the rectus femoris to maintain forward propulsion and stability. The activation of the rectus femoris in early stance and early swing is relatively similar between the MG and healthy cases, suggesting that the muscle's compensatory role is most pronounced during phases where vasti strength is crucial.

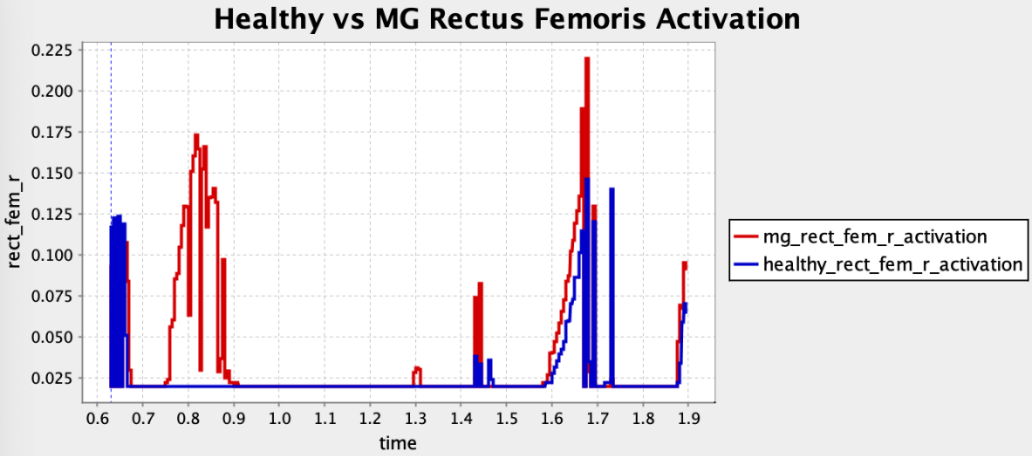


**Figure B.2.2** Comparison between the activation of the healthy and MG-impacted rectus femoris muscles

These trends are consistent with the expected behavior of the muscles under reduced Fmax conditions. The vasti, being directly affected by the pathology, demonstrate increased activations at heel strike to compensate for their loss of force-generating capacity but are unable to sustain high activations throughout the gait cycle. Meanwhile, the rectus femoris shows a distinct compensatory response in late stance, stepping in to maintain knee extension and forward progression.

### *B.3 Peak Torque*

**Figure B.3.1** compares knee joint moments for the healthy and MG cases during the gait cycle, highlighting the effects of weakened vasti muscles. In the healthy case, the knee moment peaks at ~175 Nm during mid-stance, reflecting the vasti's role in stabilizing the knee and supporting body weight. The MG case shows a reduced peak of ~90 Nm and a flatter profile, indicating a significant torque deficit and limited compensatory activity from other muscles, such as the rectus femoris.

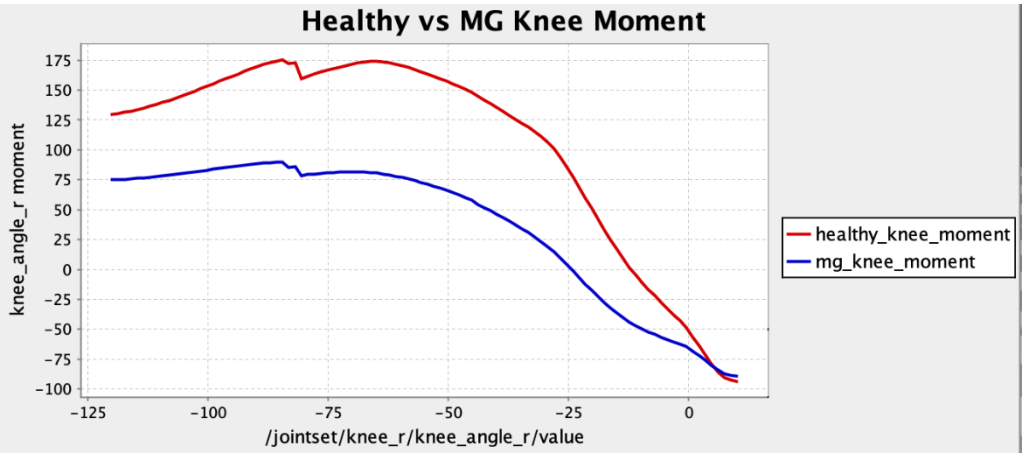


**Figure B.3.1** Comparison between the moments at the healthy and MG-impacted knees

This torque deficit (~85 Nm) during mid-stance compromises knee stability and gait efficiency. For bionic system design, these results suggest that dynamic assistance of up to 85 Nm during mid-stance is required to restore knee function and normalize gait mechanics.

# C. Bionic System for MG

The proposed bionic system is a path actuator applied at the knee joint to compensate for the reduced torque output caused by Myasthenia Gravis (MG). The system provides constant force between the tibia and the femur, acting like a linear spring and mimicking the role of the weakened vasti muscles. The device bridges the torque deficit observed in the MG case, restoring normal joint mechanics and reducing compensatory activation of the rectus femoris. Additionally, it improves energy efficiency and helps normalize the joint moment profile.

## *C.1 Bionic System Modeling*

To assist the subject in knee extension during normal gait, the team modelled a path actuator in OpenSim to compensate for the weakened vasti muscle and to reduce the load on the rectus femoris muscle. The path actuator was added to the software by running a Python script and later adjusted its placement and position within the OpenSim environment. Here, a constant activation of path actuator was assumed during the gait and all the force plots were generated accordingly. The actuator effectiveness was tested at different placement positions and for different maximum isometric forces. Based on the plots generated for the total metabolic cost for the weakened vasti muscle strength of 500N, a suitable combination of placement position and the maximum isometric force was chosen. The figures below summarize the complete activity done by path actuator for various configurations.

### *C.1.1 Lateral Placement of Path Actuator*

The path actuator as shown in **Figure C.1.1.1** below is placed parallel to the femur and the tibia and at a certain distance from the knee to account for the natural overall size of the thigh. The placement location is below in **Table C.1.1.1**.

**Table C.1.1.1** Coordinate Locations of the Path Actuator

| Bone | X Coordinate | Y Coordinate | Z Coordinate |
|---|---|---|---|
| Femur (femur_r) | -0.03 | -0.25 | 0.1 |
| Tibia (tibia_r) | -0.02 | -0.2 | 0.1 |

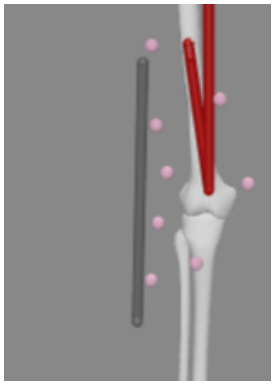

**Figure C.1.1.1** Lateral placement of the path actuator

For this particular configuration, the team tested the effect of the actuator on the forces generated by the vasti and rectus femoris during a normal gait cycle with different maximum isometric forces. These results can be seen below in **Figures C.1.1.2 through C.1.1.5**.

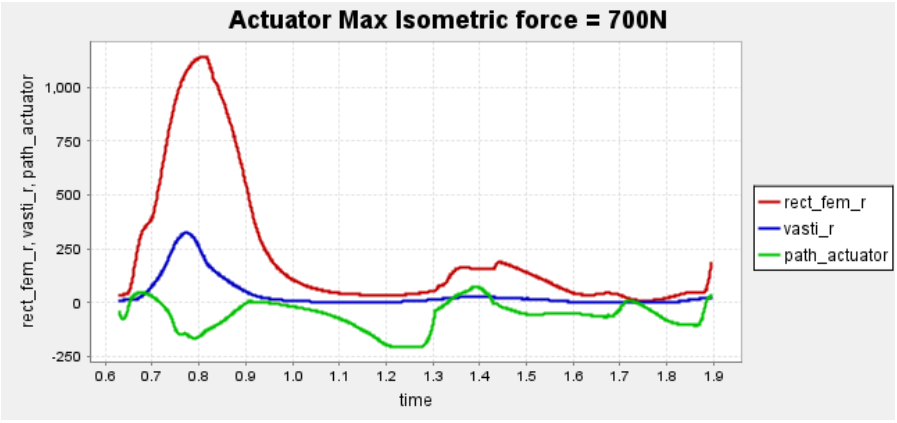


**Figure C.1.1.2** Muscle forces generated in response to a lateral actuator with a max isometric force of 700N

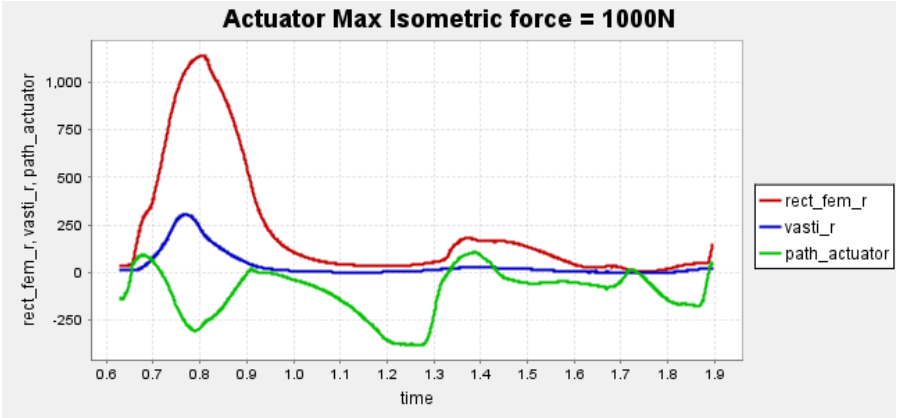


**Figure C.1.1.3** Muscle forces generated in response to a lateral actuator with a max isometric force of 1000N

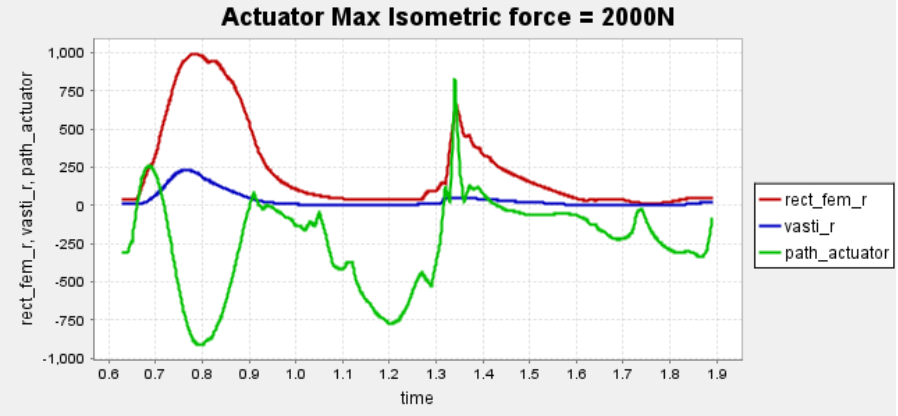


**Figure C.1.1.4** Muscle forces generated in response to a lateral actuator with a max isometric force of 2000N

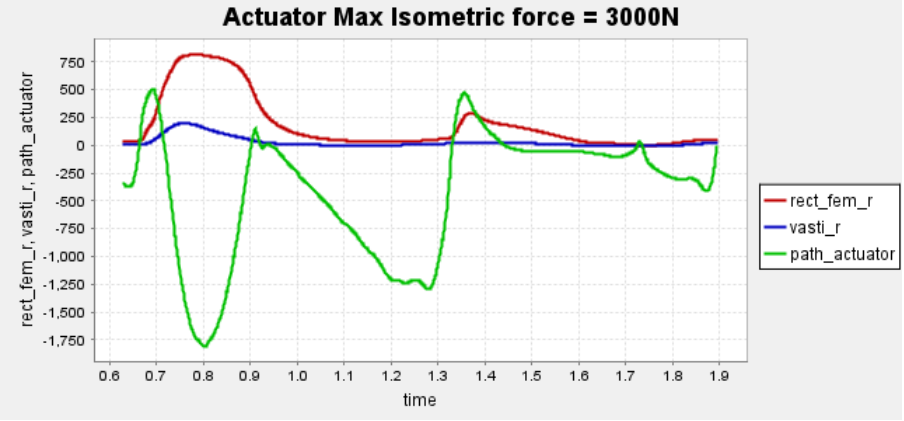


**Figure C.1.1.5** Muscle forces generated in response to a lateral actuator with a max isometric force of 3000N

### *C.1.2 Posterior Placement of Path Actuator*

The path actuator as shown in **Figure C.1.2.1** below is placed parallel to the femur and the tibia but posterior to them. The exact placement location is below in **Table C.1.2.1**.

**Table C.1.2.1** Coordinate Locations of the Path Actuator

| Bone | X Coordinate | Y Coordinate | Z Coordinate |
|---|---|---|---|
| Femur (femur_r) | -0.05 | -0.25 | 0 |
| Tibia (tibia_r) | -0.05 | -0.2 | 0 |

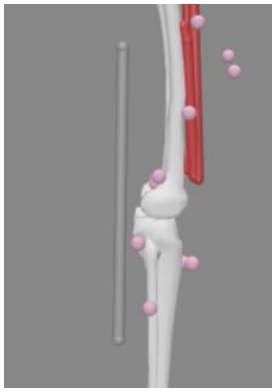

**Figure C.1.2.1** Posterior placement of the path actuator

The team tested the effect of the posterior actuator on the forces generated by the vasti and rectus femoris during a normal gait cycle with different maximum isometric forces. These results can be seen below in **Figures C.1.2.2 through C.1.2.5**.

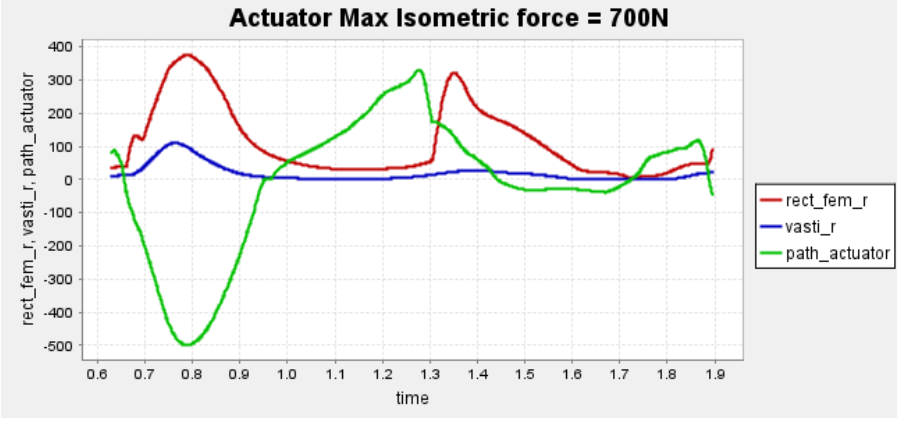


**Figure C.1.2.2** Muscle forces generated in response to a posterior actuator with a max isometric force of 700N

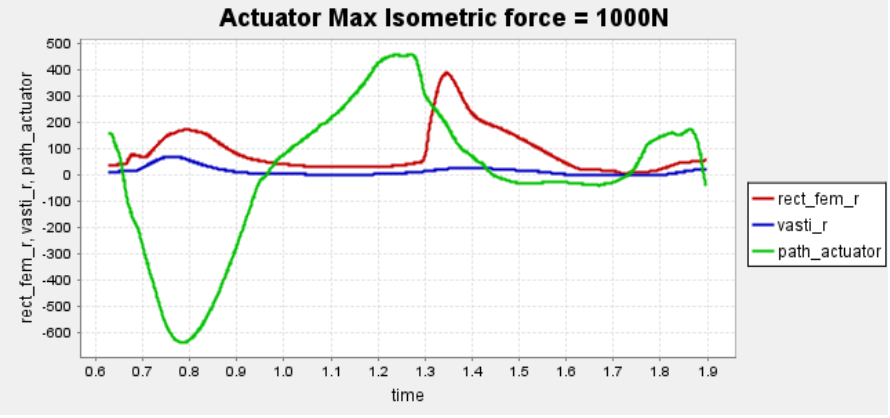


**Figure C.1.2.3** Muscle forces generated in response to a posterior actuator with a max isometric force of 1000N

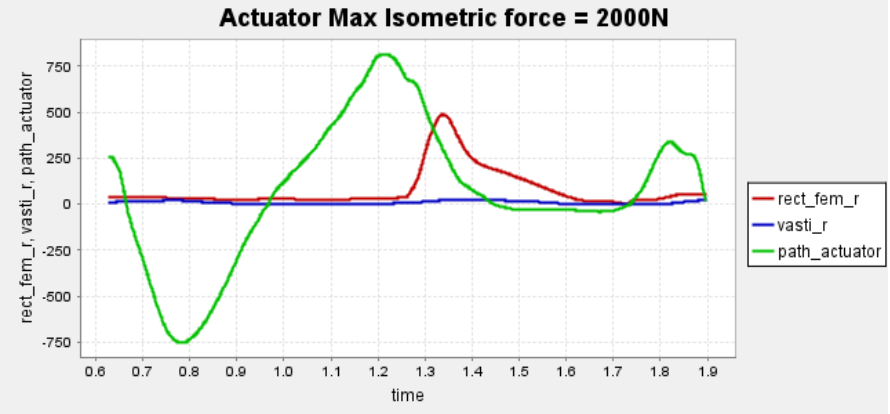


**Figure C.1.2.4** Muscle forces generated in response to a posterior actuator with a max isometric force of 2000N

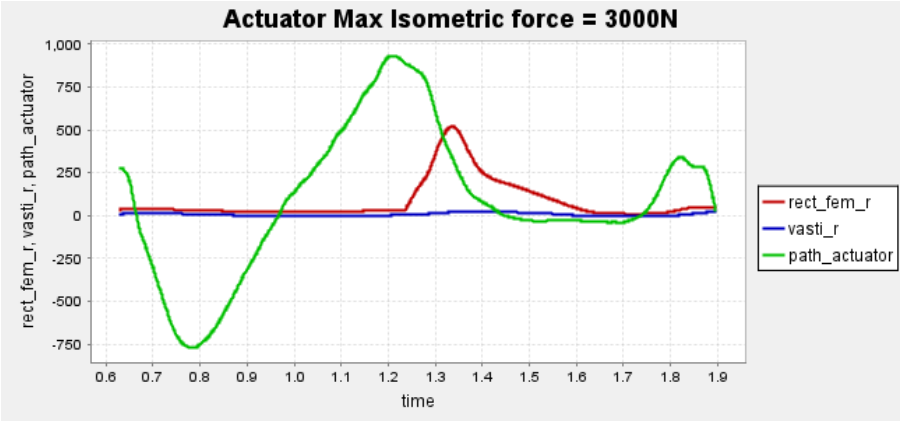


**Figure C.1.2.5** Muscle forces generated in response to a posterior actuator with a max isometric force of 3000N

When the actuator is placed on the side, it leads to an increased force requirement from the muscles, especially the rectus femoris. As the actuator is moved to the posterior placement, the force requirement of the rectus femoris is suddenly reduced which is then compensated by the actuator. Therefore, for each configuration, the team tried to increase the isometric force of the actuator. As seen from the force plots for the posterior configuration, the muscle forces for the rectus femoris are reduced. The negative forces here suggest that the actuator is pushing to assist in extension. Thus, the team optimized the actuator placement and its forces in OpenSim to yield maximum force reduction of the muscles.

### *C.2 Modeling Results Analysis*

As seen in **Figure C.1.2.4**, the muscle forces of the recuts femoris due to a posterior path actuator best match the muscle forces from a healthy subject without the bionic system, as seen in Figure **C.2.1**, when compared to the other attachment and isometric force combinations from **Section C.1**.

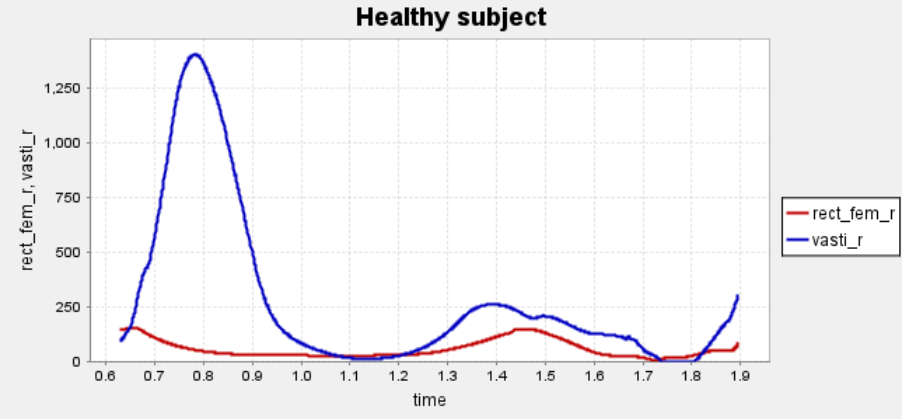


**Figure C.2.1** Vasti and rectus femoris muscle forces generated during gait by a healthy subject

The vasti muscle, during a healthy gait generates most of the force, however. After weakening it, it is expected to not generate any force and thus does not exhibit a peak in force. Hence, for the case of the weakened vasti, the path actuator compensates and generates the magnitude force peak required for the gait as seen in **Figure C.1.2.4**.

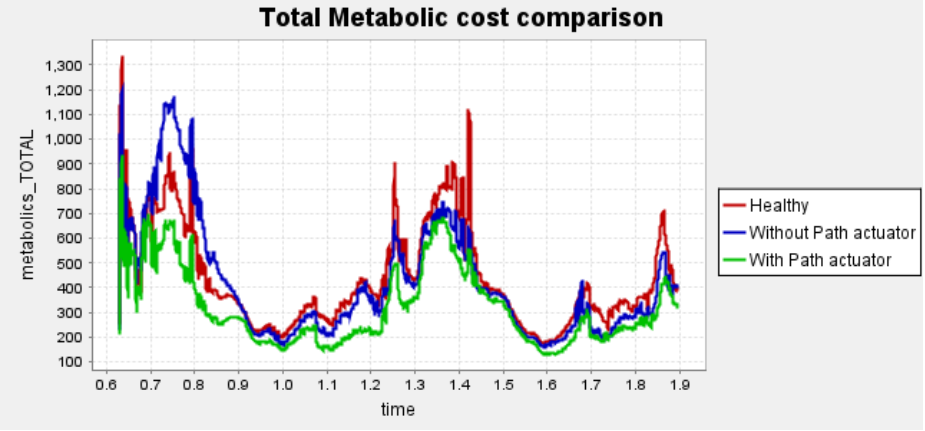


**Figure C.2.2** Total metabolic cost under various cases

Using an assistive bionic device, as seen in **Figure C.2.2**, the team was able to reduce the total metabolic cost during one gait cycle. The metabolic cost is reduced at each stage of the gait indicating the path actuator is working as expected and the subject is not burdened with the bionic system. The team was also able to reduce the peak force requirement of the rectus femoris muscle as seen in **Figure C.2.3**.

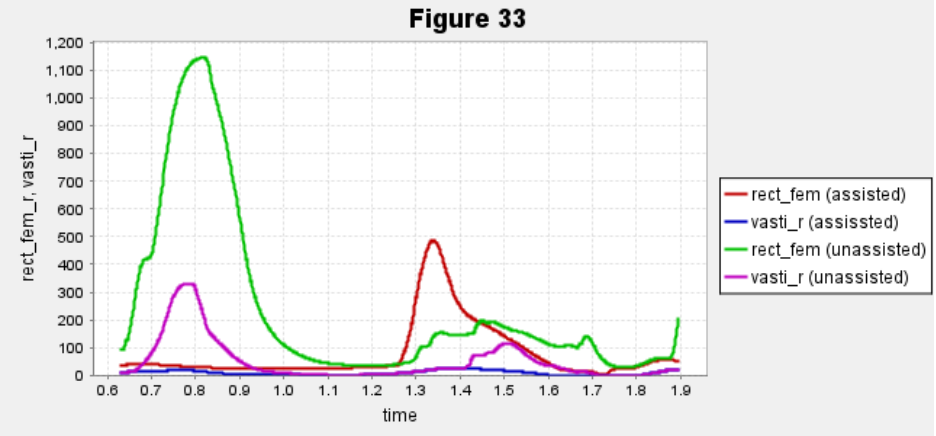


**Figure C.2.3** Peak force comparison between both muscles before and after adding the bionic system

The bionic system can be heavy, and its inertia needs to be considered while calculating the forces, torques and metabolic costs. Therefore, a conservative estimate of 3kg was made to include the prosthesis structure, electronics, motor, battery, enclosure, etc. To perform a realistic performance comparison, the team applied a mass of 2.75kg on the right femur bone and 0.25 kg on right tibia in OpenSim and compared the metabolic cost. However, there is significant potential to reduce the metabolic cost by reducing the overall weight of the system and choosing a lighter custom battery.

The data collected was dependent on the required torque trajectory. This was computed by multiplying the required forces and the moment arms during gait. The moment arms were calculated by running a custom Python script. **Figure C.2.4** shows how the moment arms vary during a gait cycle.

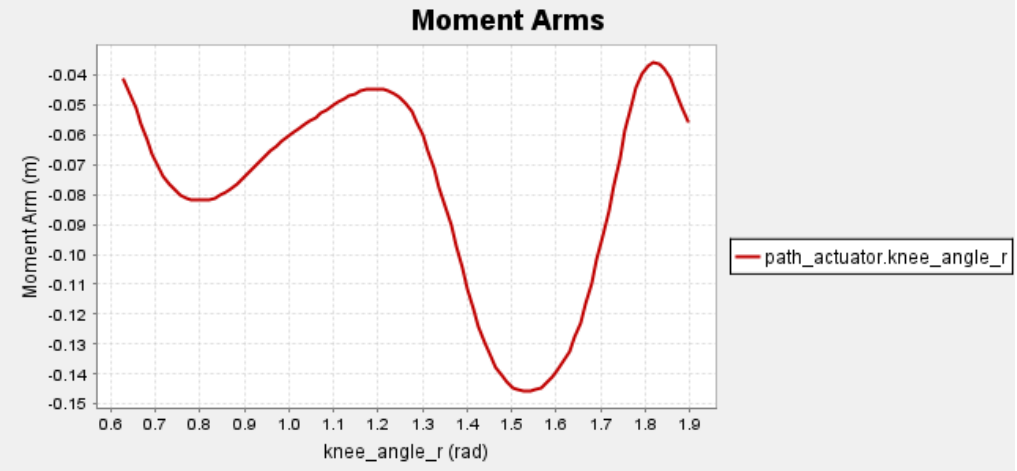


**Figure C.2.4** Path actuator moment arm vs knee angle

## D. Model Reliability (Residual Analysis)

The residual analysis, illustrated in **Figures D.1 through D.3**, evaluates the reliability of the computational model in simulating the effects of Myasthenia Gravis (MG). The lumbar extension reserve forces as seen in **Figure D.1** are significantly larger compared to the reserves at the hip, knee, and ankle joints. This is because the subject-specific model lacks sufficient musculature to stabilize the lumbar region during gait. The reserve forces for lumbar extension are essential to provide balancing forces that the model cannot generate naturally, preventing the upper body from collapsing. In contrast, the reserves for the hip, knee, and ankle joints remain within acceptable limits, indicating that these regions are well-represented by the existing musculature.

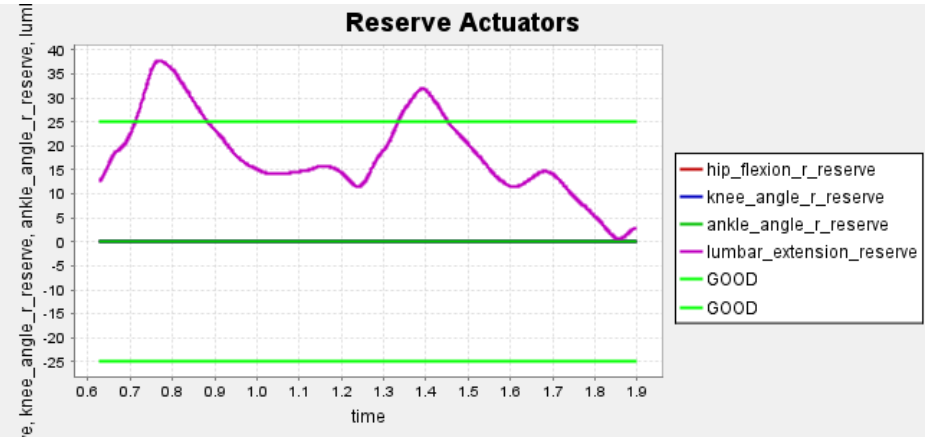


**Figure D.1** Residual analysis for reserve actuators

**Figures D.2** shows the residual forces (FX, FY) and moments (MZ) during the gait cycle. While FX and MZ stay within acceptable ranges, FY briefly exceeds the "OK" range during transitions like heel strike and toe-off. This is expected as vertical ground reaction forces (FY) are the largest and experience rapid changes during these phases. The deviations are minor and align with typical gait dynamics, indicating that the model reliably captures the overall forces, with FY's variations reflecting known limitations rather than errors.

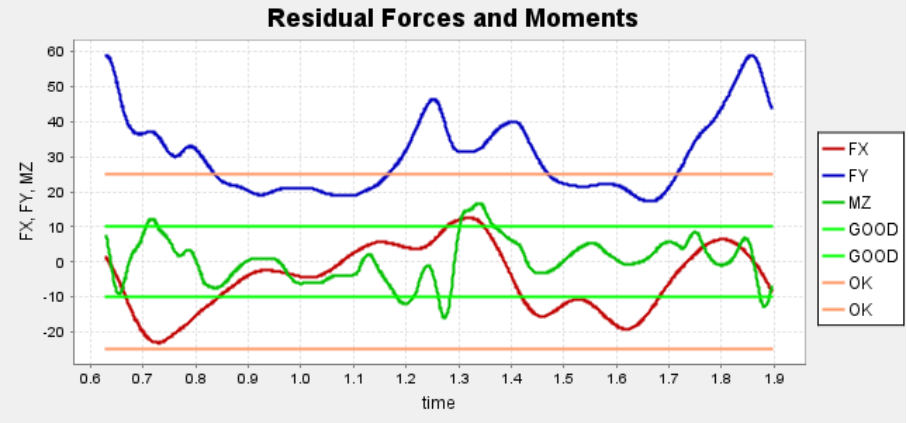


**Figure D.2** Residual analysis for residual forces and moments

**Figures D.3** presents the kinematic tracking errors, which are minimal and consistently below the threshold of 0.035 radians (~2 degrees). This demonstrates that the CMC tool effectively matched the experimental kinematics, ensuring accurate replication of joint angles throughout the gait cycle. Together, the residual forces, moments, and kinematic tracking errors confirm the reliability of the model while also highlighting limitations, such as the reliance on lumbar reserve actuators due to the absence of upper body musculature. These results validate the overall effectiveness of the model while pointing to potential improvements for future simulations.

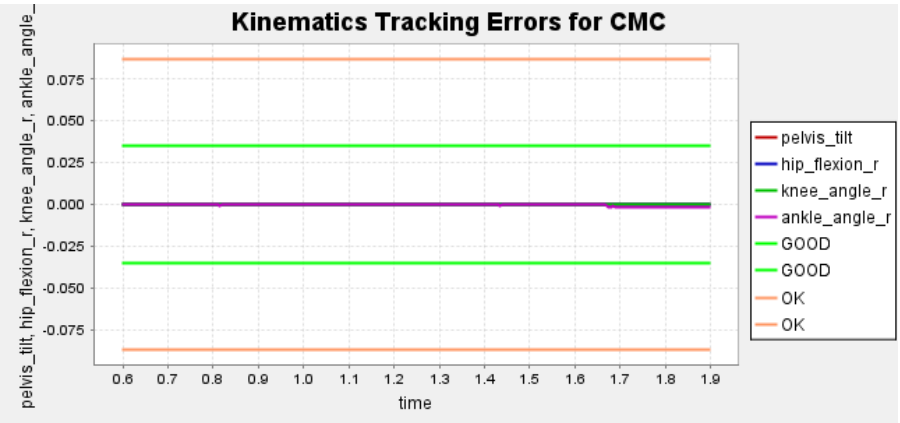


**Figure D.3** Residual analysis for kinematic tracking errors

# Section II – Bionic System Design

## E. Bionic System Overview

The proposed bionic system is an exoskeleton that attaches to the outside of the affected leg, driving the knee. It uses EMG patches to determine when the vasti is being activated and then applies torque to the knee joint via a motor and gearbox to compensate for the weaker muscle. A sketch of the system and its critical components can be seen below in **Figure E.1**.

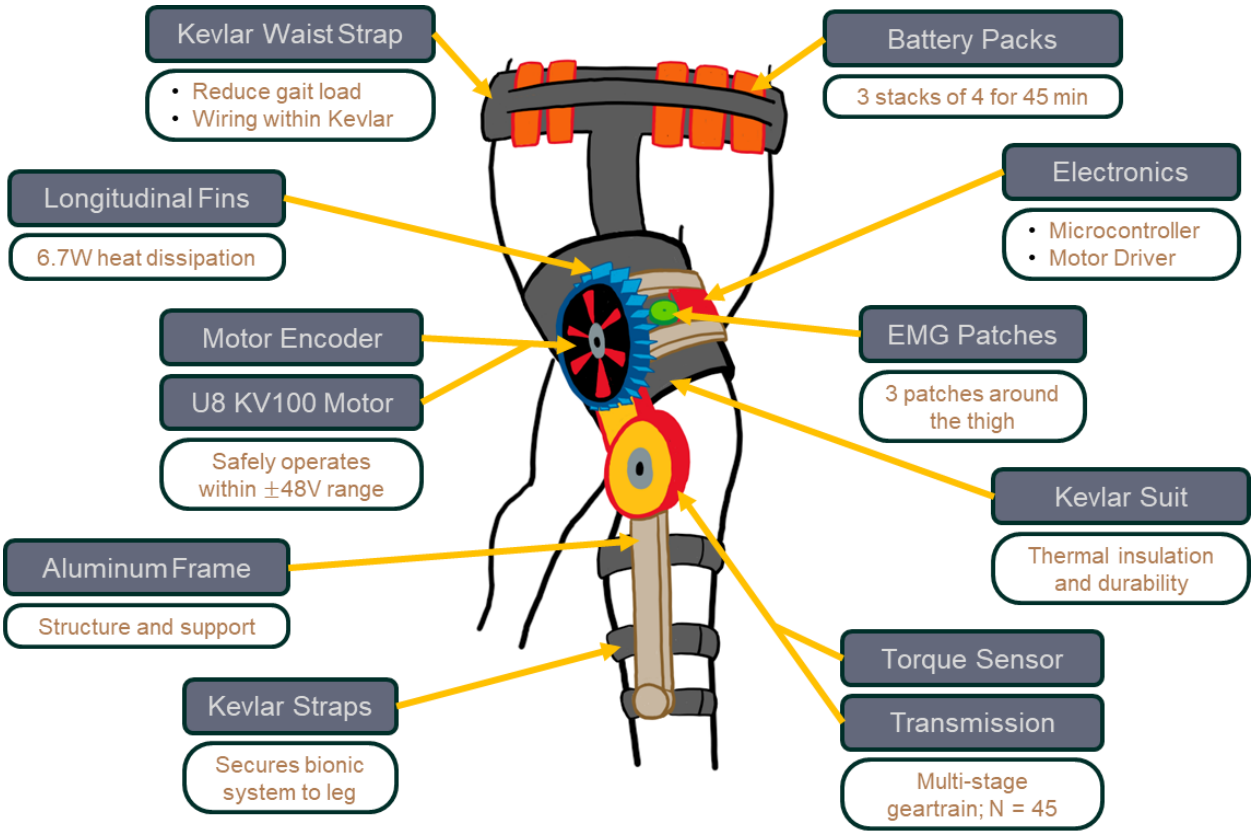


**Figure E.1** Bionic system and its critical components

## F. System Controls

The bionic system is designed to leverage the proposed communications hierarchy as seen below in **Figure F.1**. Raw EMG data is processed through the microcontroller which uses the EMG data, along with the feedback from the joint angle and motor torque to instruct the motor driver on how much current to apply to the motor and for how long in order to achieve a desired torque output.

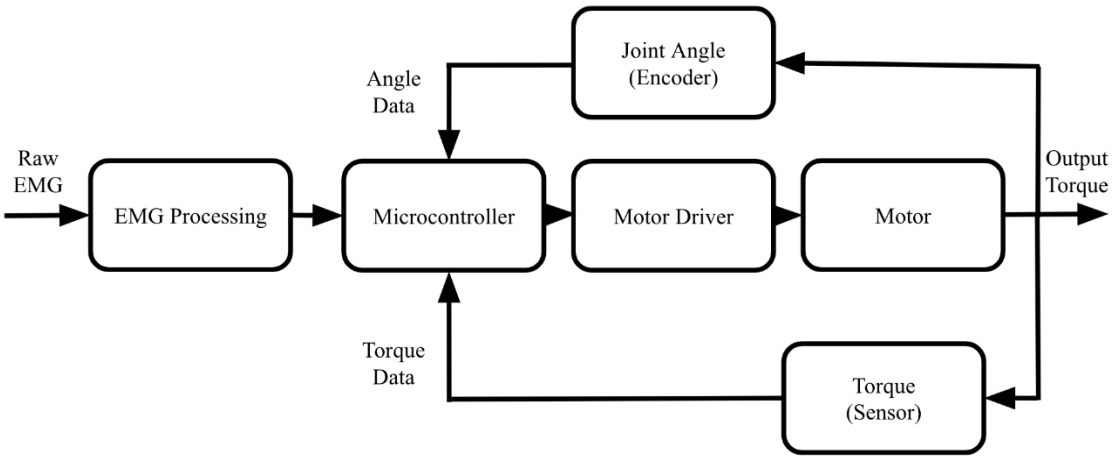


**Figure F.1** Communications Hierarchy

### *F.1 High Level Control*

The high-level control system uses electromyography (EMG) signals to detect the activation patterns of the vasti muscle. By sensing these signals, the system then determines when to apply torque and how much to apply. The control system determines that torque should be applied when the vasti muscles are activated, such as during knee extension in the gait cycle. The amount of torque the motor should generate is calculated based on the magnitude of the EMG signal amplitude.

### *F.2 Mid-Level Control*

The mid-level control bridges the high-level EMG detection system with the mechanical actuation of the exoskeleton. It includes gait phase detection, torque profiles, and safety monitoring. For gait phase detection, the system uses an encoder, a torque sensor, and muscle activation data to identify the user's current gait phase and adjusts torque application accordingly. The gait phase, along with EMG signals, affects the torque profile. Smooth torque profiles are implemented to ensure natural knee motion. Lastly, the system includes real-time monitoring of the knee joint angle and torque to ensure the applied torque does not exceed safe limits or cause discomfort to the user.

### *F.3 Low Level Control*

The low-level control handles details of the motor actuation, ensuring the precise application of torque in accordance with the mid-level system. It includes three primary features: motor control, feedback loops, and stability algorithms. A microcontroller communicates with the motor driver to ensure accurate motor torque output and smooth operation. The angle and torque output is then recorded by a joint encoder and torque sensor, respectively, to provide real-time feedback and adjust the motor's performance, compensating for unexpected variations in load torque. In addition, the microcontroller also uses PID control to smoothly and efficiently actuate the motor. It also has other built-in algorithms to detect anomalies like excessive resistance which trigger fail-safes such as torque reduction.

### *F.4 Component Selection*

A Raspberry Pi 5 will be used as the microprocessor. As for the motor driver, a Cytron MD20A will be able to supply the required current and voltage to the motor. An incremental rotary encoder will be used to record the joint angle, down to the degree. Finally, the torque sensor will be a Futek B5 Torque Sensor. These components are shown below in **Figure F.4.1**.

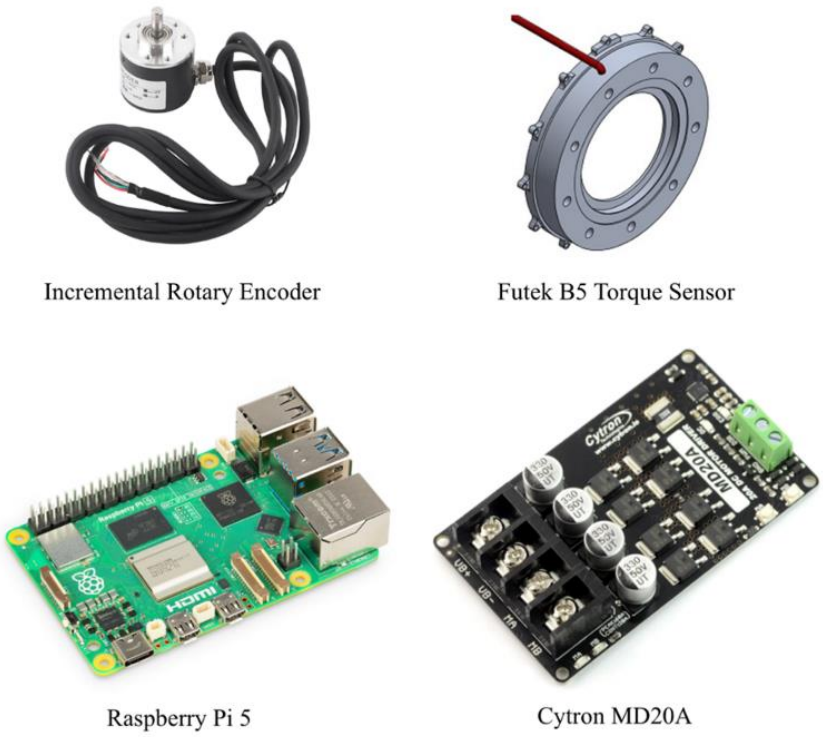


**Figure F.4.1** Controls Components

## G. Desired Torque and Angle

The required torque for the system is calculated through the product of forces (derived after running the CMC with the desired actuator) and the moment arms (See Figure C.2.4). This product is then plotted against time to get torque requirements for the bionic system. The generated torque data drove the design requirements of the bionic system along with the motor selection. The absolute peak torque to be generated by the bionic system is 63.2 Nm in magnitude as seen in **Figure G.1**.

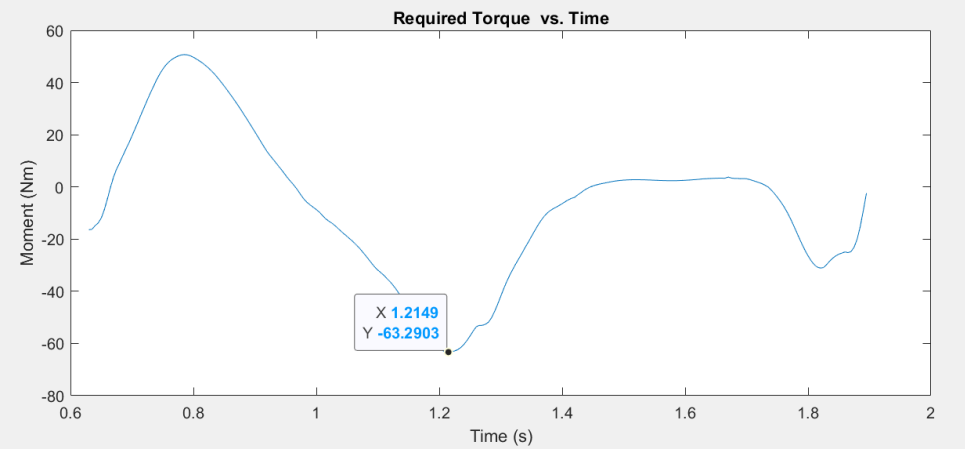


**Figure G.1** Maximum torque required can be seen at around t = 1.2 seconds in the gait cycle

The knee angle plot, as seen in **Figure G.2**, describes the range of angles the knee traverses during a gait cycle and thus impacted the team's decisions on the placement of the bionic system on the leg.

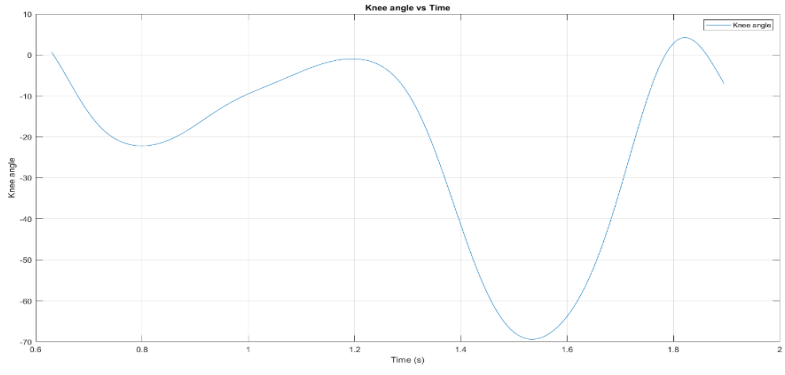


**Figure G.2** Knee angle required changes over time throughout the gait cycle

## H. Actuator Design

The U8 KV100, a brushless motor produced by the company T-motor, as seen below in **Figure H.1**, is suitable for use in the exoskeleton. It is a "pancake" motor intended for use in large drones but can also be used in the proposed application. The motor runs at 48V, has a diameter of 87.3 mm and a thickness of 26.05 mm. The "pancake"-like geometry allows the motor to lie flat along the side of the exoskeleton and interface with the custom gear box.


**Figure H.1** A U8 KV100 motor

The specifications of this motor were loaded into a MATLAB script, along with the required torque and angle trajectories, to generate a plot of the current and voltage requirements for the motor in order for it to produce the desired torque-position trajectory. This data can be seen below in **Figure H.2**.

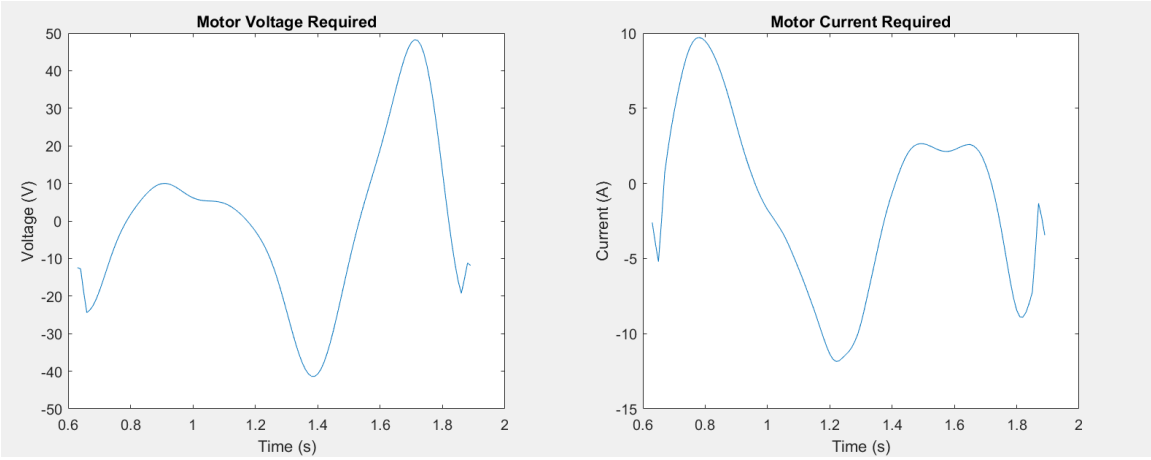


**Figure H.2** Voltage and current requirements for the proposed motor to meet the desired torque-position trajectory

The specifications considered included the motor inertia, torque constant, resistance and inductance. The team assumed a standard efficiency of 85% and tested various transmission ratios until the electrical requirements were within reason: the voltage needed to be low enough to fit within the proposed battery's ideal operating limits and the current needed to be low enough to minimize power loss and maximize efficiency. As seen below in **Figure H.3**, various motors had been tested along a range of transmission ratios to find the optimal combination. The U8 KV100 motor stood out for its performance in minimizing power loss while still meeting torque requirements.

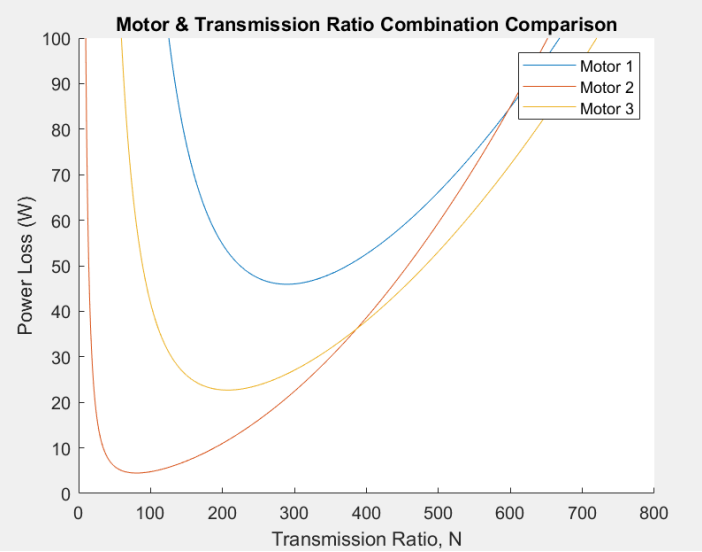


**Figure H.3** The U8 KV100 (Motor 2) being tested against other motors along a range of transmission ratios

Though the minimum power loss for this motor was at a transmission ratio of $N = 80$, this increased the voltage range and thus would lead to the motor overheating and more inefficiencies. The team thus decided that a trade-off was necessary, and it would be worth sacrificing the 2.2W of power loss from a lower transmission ratio in exchange for much better performance and efficiencies due to optimal motor performance and a lack of overheating. At a transmission ratio of $N = 45$, the voltage limits were within a $\pm 48V$ range – the standard operating spectrum for LiPo batteries the team was considering. The electrical performance at this transmission ratio is what is depicted above in **Figure H.2**.

### *H.1 Transmission System Design*

To achieve the desired transmission ratio of $N = 45$ and meet the torque trajectory, the motor needed to be coupled with a transmission system. This was done using a multi-stage gear train system with gear ratios of 5:1 and 9:1. Each stage contributed to the overall reduction, with the total transmission ratio calculated as the product of the individual ratios:

$$N = 4.5{:}\,0.5 * 5{:}\,1 = 45{:}\,1$$

The first stage applies a 5:1 ratio, increasing torque output by 5 times, while reducing the speed proportionally. The second stage, with a 9:1 effective ratio, further multiplies the torque to reach the desired output of 63.2 Nm, matching the trajectory requirements. This two-stage design is compact, efficient, and distributes the load across stages to prevent excessive wear on individual components.

### *H.2 Heat Dissipation*

As explained earlier, a slightly inefficient transmission ratio was chosen to optimize the entire system's efficiency. As a result, the average power loss is around 6.7W as previously seen in **Figure H.3**. This power loss is most likely released as heat and thus needs to be dissipated to avoid overheating and discomfort to the user. Overheating can also increase motor inefficiency.

To dissipate the heat being generated at a rate of 6.7W, the motor's gearbox will have external fins, which increase the surface area available for heat transfer via convection. These fins will allow the system to effectively release thermal energy into the surrounding air, preventing overheating during operation. By maintaining an optimal temperature range, the fins ensure consistent performance and extend the lifespan of the motor and gearbox components. Furthermore, as seen in **Section E**, the bionic system incorporates Kevlar in its suit to create a durable and insulative layer between the motor and the user in order to reduce heat transfer and reduce discomfort.

# I. Adding a Series Elastic Actuator

To test the effectiveness of adding a series elastic actuator (SEA) to the proposed prosthesis, three transmission ratios in question were selected to be compared. At each of the three ratios, the power loss was computed for all SEA stiffnesses ranging from 10 to 1000, as seen in **Figure I.1**.

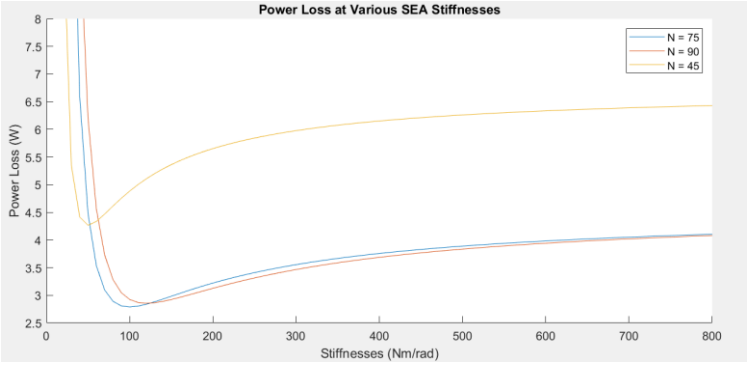


**Figure I.1** Optimizing for SEA stiffnesses by power loss at various transmission ratios

The SEA stiffness with the lowest minimum power loss was selected for each transmission ratio. The optimal transmission ratio was then chosen based on if the voltage and current requirements at that SEA stiffness and transmission ratio were within the engineering requirements and capabilities of the selected motor. In this case, the optimal transmission ratio was the same with or without a SEA: $N = 45$. Despite this transmission ratio not yielding the lowest power loss and current requirements, it was still selected as optimal due to its lower voltage requirements as seen below in **Figure I.2**.

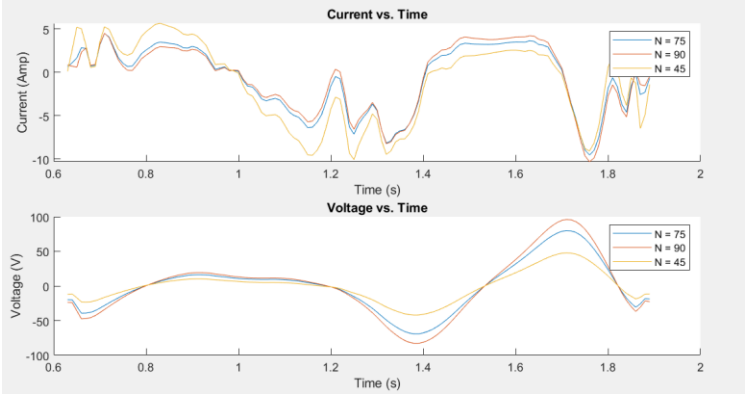


**Figure I.2** The SEA at $N = 45$ has larger current but lower voltage requirements and thus was chosen as optimal

At this transmission ratio, the ideal SEA stiffness was 50 Nm/rad. Such an elasticity could be implemented through a compliant mechanism or a torsional spring. Carbon fiber flexures or spring steel torsional springs are both great options due to their strength, durability, resistance to fatigue, and weight.

Once an optimal SEA stiffness and transmission ratio combination was chosen, it was important to check if installing this SEA would be beneficial in comparison to not having a SEA. A SEA in this application should help reduce current requirements and improve efficiency as the system would store and release energy during push-off and knee-extension, boosting gait performance and aiding with shock absorption. A damaged vasti would thus benefit from a SEA. This hypothesis was proven correct by the data found in **Figure I.3**. A SEA with a stiffness of 50 Nm/rad at a transmission ratio of 45 for the selected motor improved performance.

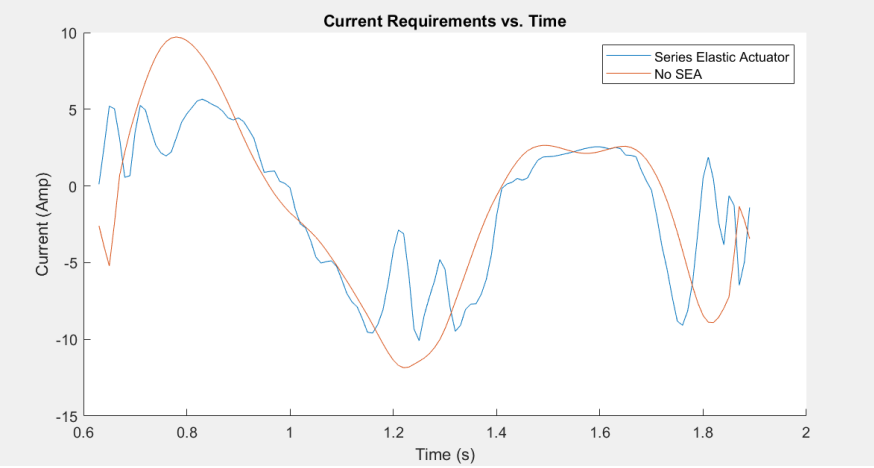


**Figure I.3** An SEA reduces current requirements and improves performance

## J. Power Requirements and Battery Selection

The selected motor functions at 48V and needs to be able to draw up to 11A. An array of 13 3.7V 1080 mAh High-Rate Discharge LiPo batteries connected in series will provide 48.1V and 1080 mAh. The weight of the battery array will be 325g. Because they are rated for high discharge with a C value of 15, this array can output a maximum continuous discharge of 16.2A.


**Figure J.1** A High-Rate Discharge LiPo Battery

In order to find the total runtime of the system, the average power consumption needed to be found. A comparison between the power input and power loss during the gait cycle can be seen below in **Figure J.2**.

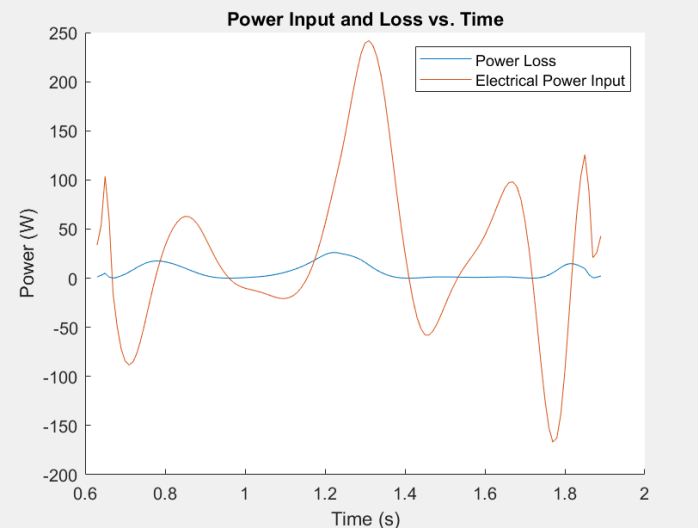


**Figure J.2** Power input vs. loss for the bionic system during the gait cycle

With a capacity of 1080 mAh, the proposed battery array will be able to provide power for approximately 46 minutes of standard gait walking, based on the average power consumption from the simulation and the following runtime ($t_{total}$) equation:

$$t_{total} = \frac{E}{P_{input_{avg}}} = \frac{48V \cdot 1080\ \text{mAh}}{62W} = 0.774\ \text{hrs} = 46.45\ \text{min}$$

A runtime of 46 minutes is adequate for an exoskeleton because it aligns with typical usage scenarios as the average American only walks for 30 minutes per day. This duration allows many patients to perform targeted activities such as rehabilitation or small hikes. Additionally, the short runtime minimizes the weight of the battery pack, improving the overall comfort and usability of the exoskeleton. If longer runtimes are required, battery arrays can be swapped or added due to the expandable nature of the bionic system's battery housing on the waist band. For example, a 2160 mAh battery array can easily be incorporated to extend operational time by doubling the number of LiPo cells.

## K. Attachment System

The bionic system is an exoskeleton that attaches around the waist, thigh, and calf via a Kevlar suit. The waistband houses battery packs for the system to alleviate weight from the legs and allow the hips to bear it instead. Furthermore, by equally distributing it across the hip and not keeping the battery packs on the injured leg, weight discrepancies between the legs are avoided. An unequal mass distribution could induce irregular gait and discomfort.

Velcro straps are also incorporated into the Kevlar suit at the thigh and calf. This allows the user to adjust the tightness as necessary, in a weight-efficient manner, ensuring fit and comfort. This proposed attachment strategy can be seen below in **Figure K.1**.

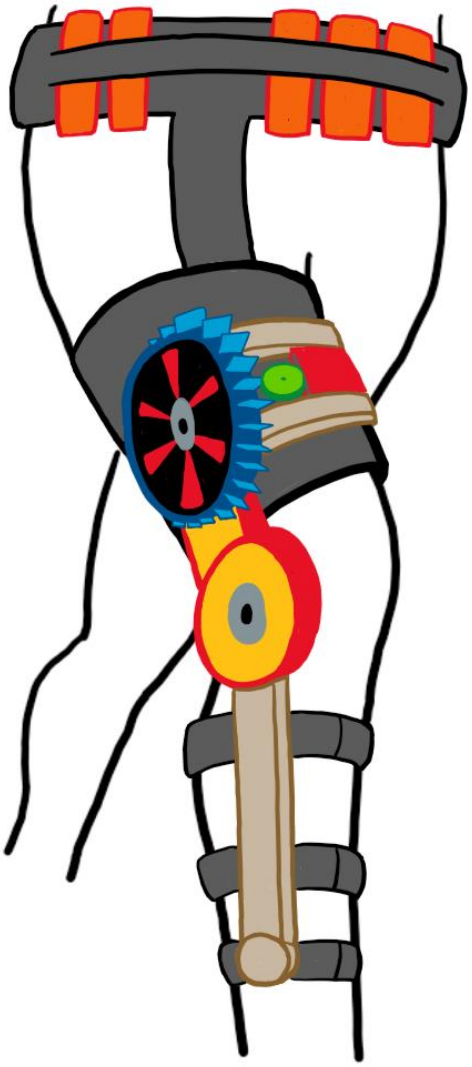

**Figure K.1** Bionic system attachment system

## L. Mass and Torque Density

The initial total weight of the system was assumed to be 3 kg with 2.75 kg weight added above the knee and 0.25 kg added on the tibia. However, after finalizing the components to be used in the actual bionic system, the total weight was about 1.75 kg. This weight was distributed as 1.5 kg above the knee and 0.25 kg on tibia. The entire simulation was then rerun with the true weight of the bionic system to identify the effects of the system's weight. This change in weight and associated load torque from the system had a negligible impact on the new metabolic cost, or the forces generated by the vasti and rectus femoris as seen in **Figures L.1 through L.2**.

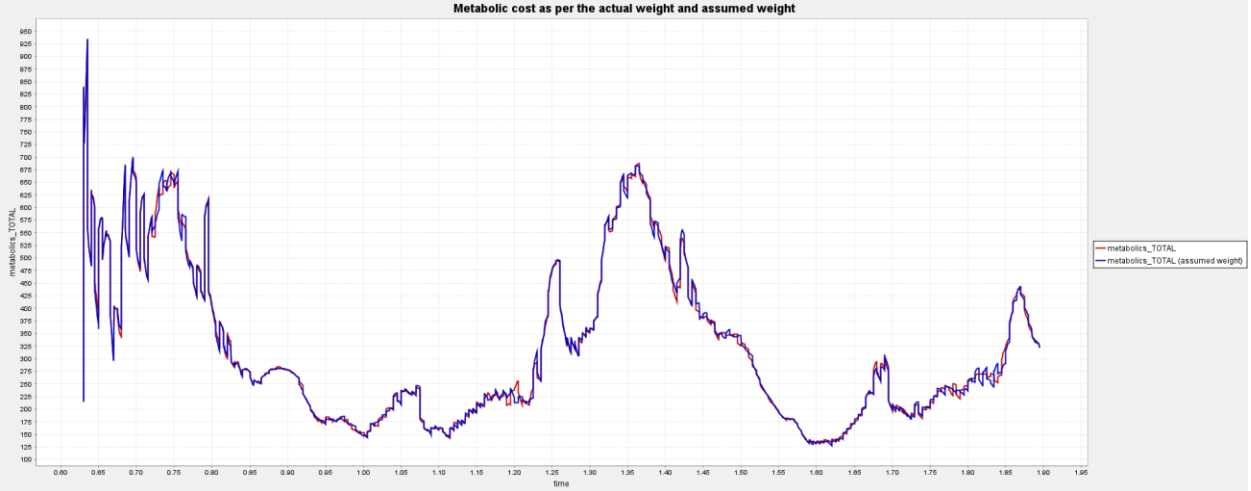


**Figure L.1** Metabolic cost comparison due to the assumed and true bionic system weight

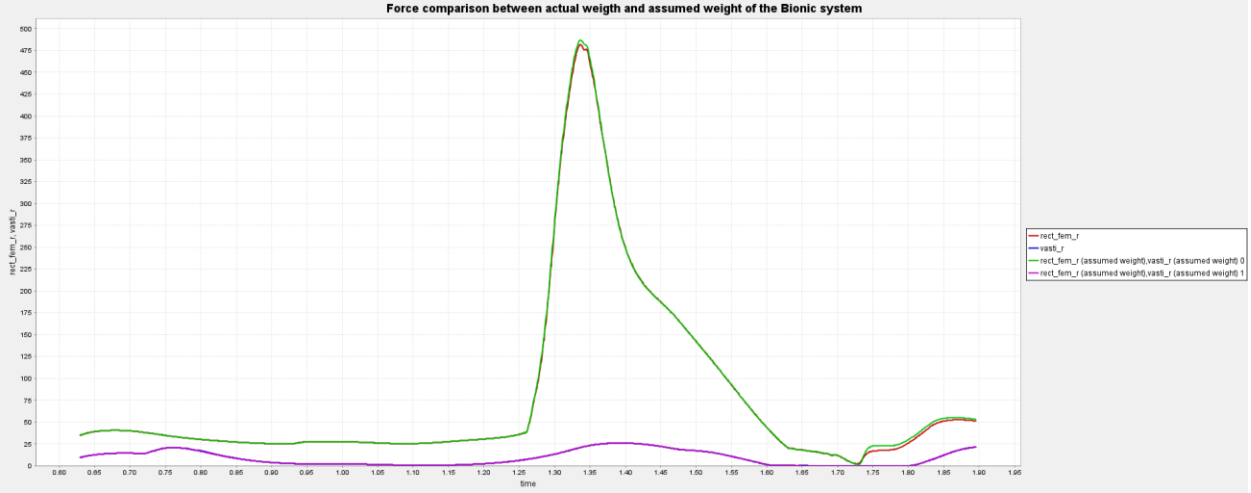


**Figure L.2** Forces generated by the vasti and rectus femoris muscles due to assumed vs true bionic system weight

The figures above show that the effects of a change in weight of the bionic system have little impact on metabolic cost. Moreover, it shows that more weight can be added above the knee, especially batteries for extended usage, without creating significant impact on the metabolic cost and the generated forces. The weight on the tibia can only be changed slightly as any larger changes could lead to different torque requirements that the designed bionic system isn't optimized to handle effectively.

As seen earlier in **Figure G.1**, the peak torque requirement was around 63.2 J. Given that the new mass of the system is 1.7 kg, the torque density can be found as a ratio of the peak torque and mass of the system: 37 J/kg.

# Section III – Anatomical Engineering

## M. Surgical Method

The current, noninvasive bionic solution leverages topical electrodes to read electromyography (EMG) data. However, Myasthenia Gravis affects the neuromuscular junction, inhibiting the nerve impulses from reaching a muscle in the first place. Thus, EMG signals from an impacted muscle would be very weak and inaccurate, leading to poor input for the bionic system to respond to.

To resolve this, an invasive surgical method can be implemented to read the signals directly from the nerve. Electroneurography (ENG) will better capture the nerve activity and intended electrical signals. However, one of the downsides is that ENG signals are harder to read, process, and interpret.

To allow the exoskeleton to interface with the user's nervous system, the team proposes surgically implanting an interfascicular electrode into the femoral nerve. This implantation method was chosen for its balance between invasiveness and effectiveness as compared to other methods as seen below in **Table M.1**.

**Table M.1** Comparison between various ENG implantation methods

| Electrode Type | Benefits | Drawbacks |
|---|---|---|
| Extrafasicular | Less invasive, durable, simple, reduced chance of nerve damage | Low selectivity, higher activation threshold, increased noise |
| Intrafasicular | Higher selectivity, lower activation thresholds, better signal fidelity | Invasive, risk of nerve damage/scarring, shorter lifespan, complex implantation |
| Sieve | Highly selective, bidirectional, aids with nerve regeneration | Highly invasive, risk of regeneration failure, complexity, longer recovery |

The implantation procedure involves a minimally invasive approach under general anesthesia. The femoral nerve is exposed through a small incision in the upper thigh, and a high precision interfascicular electrode is carefully inserted into the nerve's fascicles to target motor fibers specifically associated with the vastus muscle. The electrode is designed to record neural activity which is then communicated to the microcontroller on the exoskeleton. Using this data, the microcontroller interprets the signal and, using preset algorithms along with data from the encoder and torque sensor, tells the motor driver how to actuate the motor.

## N. Cost-Benefit Analysis

The implantation of an interfascicular electrode comes with many health-related risks. These risks include infection, nerve damage, and electrode displacement. If proper sanitization protocols are not followed, bacteria from the procedure could lead to infection within the incision. This could lead to dangerous complications. The electrode will be implanted within the nerve, which could result in unfortunate damage. This could have a cascade effect, ultimately leading to partial or complete loss of control of muscles further down from where the nerve is damaged, but the probability of this occurring is less than 5%. Additionally, the electrode could displace due to fibrosis, resulting in a weaker ENG signal. If the electrode displacement is significant enough, the sensor could completely disconnect from the nerve, rendering the procedure useless. The likelihood of this occurring is less than 10%. The patient will also have a visible scar on the thigh and the patient would have spent over 100 hours through the operation, recovery, training, and checkups from this procedure.

The overall success rate of this procedure, however, is around 85% and can offer significant benefits. Enhanced mobility and independence are key outcomes, reducing reliance on others while also preventing secondary health issues like joint stiffness and muscle atrophy. The intuitive nature of the control system improves the user's experience, requiring less cognitive effort to operate the exoskeleton. There are also potential psychological benefits of this procedure and system, such as increased confidence and social engagement. In the long term, this intervention can offset its initial costs by reducing healthcare expenses and enabling some users to regain productivity, making it a transformative solution for those with debilitating Myasthenia Gravis in their vastus muscle.

While there are risks, the minimally invasive nature of the procedure and its long-term benefits of improved mobility allow the benefits of this procedure to outweigh the costs. This procedure should be recommended for those whose vasti muscles are severely affected by MG as it allows the user to gain greater control over the exoskeleton. By directly interfacing with the femoral nerve via an interfascicular electrode, the system achieves precise control of the exoskeleton which compensates for the weakened vastus muscle. This level of integration significantly enhances the user's mobility and quality of life.

## References

[1] Myasthenia gravis. (2023). Retrieved from https://www.mayoclinic.org/diseases-conditions/myasthenia-gravis/symptoms-causes/syc-20352036

[2] Suresh, A. B. (2023). Myasthenia Gravis. Retrieved from https://www.ncbi.nlm.nih.gov/books/NBK559331/#:~:text=Myasthenia%20gravis%20(MG)%20is%20the,eyes%2C%20throat%2C%20and%20extremities.

[3] Aashit K Shah, M. (2024). Myasthenia Gravis. Retrieved from https://emedicine.medscape.com/article/1171206-overview?form=fpf